3D Subject-Specific Shape and Density Estimation of the Lumbar Spine from a Single Anteroposterior DXA Image Including Assessment of Cortical and Trabecular Bone

Mirella López Picazo*, Alba Magallón Baro, Luis M. del Río Barquero, Silvana Di Gregorio, Yves Martelli, Jordi Romera, Martin Steghöfer, Miguel A. González Ballester, and Ludovic Humbert

Abstract— **Dual Energy X-ray Absorptiometry (DXA) is the standard exam for osteoporosis diagnosis and fracture risk evaluation at the spine. However, numerous patients with bone fragility are not diagnosed as such. In fact, standard analysis of DXA images does not differentiate between trabecular and cortical bone; neither specifically assess of the bone density in the vertebral body, which is where most of the osteoporotic fractures occur. Quantitative Computed Tomography (QCT) is an alternative technique that overcomes limitations of DXA-based diagnosis. However, due to the high cost and radiation dose, QCT is not used for osteoporosis management. We propose a method that provides a 3D subject-specific shape and density estimation of the lumbar spine from a single anteroposterior (AP) DXA image. A 3D statistical shape and density model is built, using a training set of QCT scans, and registered onto the AP DXA image so that its projection matches it. Cortical and trabecular bone compartments are segmented using a model-based algorithm. Clinical measurements are performed at different bone compartments. Accuracy was evaluated by comparing DXA-derived to QCT-derived 3D measurements for a validation set of 180 subjects. The shape accuracy was 1.51 mm at the total vertebra and 0.66 mm at the vertebral body. Correlation coefficients between DXA and QCT-derived measurements ranged from 0.81 to 0.97. The method proposed offers an insightful 3D analysis of the lumbar spine, which could potentially improve osteoporosis and fracture risk assessment in patients who had an AP DXA scan of the lumbar spine without any additional examination.**

*M. López Picazo is with *BCN Medtech, Universitat Pompeu Fabra*, 08018 Barcelona, Spain and with *Galgo Medical S.L.*, 08036 Barcelona, Spain (correspondence e-mail: mirella.lopez.picazo@gmail.com). A. Magallón Baro, Y. Martelli, J. Romera, M. Steghöfer and L. Humber are with *Galgo Medical S.L.*, Barcelona, Spain. L. M. del Río Barquero and S. di Gregorio are with *CETIR Grup Mèdic*, Barcelona, Spain. M. A. González Ballester is with *BCN Medtech, Universitat Pompeu Fabra,* Barcelona, Spain and with *ICREA,* Barcelona, Spain.
This paper contains supplementary materials and color versions of the figures available online at http://ieeexplore.ieee.org in the supplementary files /multimedia tab.

Index Terms— **Bone mineral density, cortical thickness, DXA, image registration, lumbar spine, statistical model**

I. INTRODUCTION

OSTEOPOROSIS is defined as "a systemic skeletal disease characterized by low bone mass and microarchitectural deterioration of bone tissue with a consequent increase in bone fragility and susceptibility to fracture" [1]. It is the most common bone disease: approximately 22 million women and 5.5 million men older than 50 years are estimated to have osteoporosis in the EU [2]. The absence of symptoms in the early stage leads to millions of people remaining undiagnosed and untreated [3], increasing their probabilities to suffer from a fracture. Worldwide, 1 in 3 women and 1 in 5 men aged over 50 years old experience osteoporotic fractures [4], [5].

The World Health Organization recommends the evaluation of Bone Mineral Density (BMD) to diagnose osteoporosis [6], [7]. The BMD is used to calculate the T-score as: the difference between the patient's BMD and the mean BMD of a reference young healthy population, divided by the standard deviation of the reference population. Postmenopausal women and men age 50 years and older are diagnosed with osteoporosis when their T-score measured at the lumbar spine, total hip, or femoral neck is ≤ -2.5 [8].

Dual Energy X-ray Absorptiometry (DXA) is the most used technique to evaluate BMD, as it is a low radiation, painless and non-expensive technique. DXA provides 2D images in which the areal bone mineral density (aBMD, g/cm^2) is measured. The International Society for Clinical Densitometry (ISCD) recommends to use the projected density along the anteroposterior (AP) direction to diagnose osteoporosis at the lumbar spine [8]. Vertebral fractures mainly take place in the vertebral body [9]. However, in AP DXA scans of the lumbar spine, the vertebral bodies superimpose with the posterior part of the vertebrae (pedicles, spinous processes and facets). Therefore, the vertebral body BMD cannot be estimated in AP DXA scans without including the posterior part of the vertebra, which is a limitation of DXA-based diagnosis of osteoporosis at the lumbar spine. Bone strength and fracture risk do not only depend on BMD but also on bone quality

[10]. Whereas low aBMD is among the strongest fracture risks [11], it is not sufficient to explain all osteoporotic fractures [12]. In fact, low aBMD only explains 60 to 80 % of bone strength under laboratory conditions [13], and only 50 % of osteoporotic fractures are observed in postmenopausal women with a T-score below -2.5 [14]. Trabecular bone architecture and cortical bone thickness are important elements that determine bone quality [15]. In osteoporotic bones, trabecular and cortical volumetric BMD (vBMD) decrease (with different rates), as trabecular bone becomes more porous and cortical bone thickness decreases [16]. Trabecular and cortical bone have different metabolic processes and response to medication [17]. However, trabecular and cortical tissues are difficult to assess separately in a DXA scan.

An alternative technique to measure BMD is Quantitative Computed Tomography (QCT). QCT uses a standard CT scanner with a calibration phantom to convert Hounsfield Units of the CT image to BMD values. Using this technology, a 3D analysis of the bony structure can be performed, vertebral body vBMD can be measured independently of the posterior part of the vertebra, and even trabecular or cortical structures can be evaluated separately. However, QCT results in exposure to a higher dose of radiation and is more expensive, compared to DXA. Moreover, cortical thickness (especially at the vertebral body) has dimensions in the range of the spatial resolution of clinical QCT scans and thin cortices need advanced techniques to be measured accurately [18]. Consequently, QCT is rarely used in clinical practice for osteoporosis management [16].

To overcome the limitations of DXA and QCT, methods using statistical models and registration algorithms were proposed to estimate the 3D shape and density of bones from a limited number of DXA scans. Statistical Shape Models (SSM), proposed by Cootes [19], capture statistical shape variability of anatomical structures within a population from a training dataset. Statistical Appearance Models (SAM) [20] capture grey-level appearance, allowing to characterize the inner structure of the objects. Active Shape and Appearance Models register and fit the SSM and SAM, with the aim to characterize and interpret similar structures in new data.

SSMs, generated from CT images, are used to recover the 3D shape of the proximal femur from a few radiographs [21]–[23]. Individual vertebral SSMs are used to estimate 3D subject-specific scoliotic spines from posterior-anterior and lateral radiographs [24], [25]. These methods focus on estimating the 3D bone shape from 2D images. Other methods are proposed to estimate, in addition to bone shape, the BMD distribution, [26]–[28].

However, in the above-described methods, no specific algorithm is proposed to quantify the cortical and the trabecular bone. Väänänen *et al*. [29] rely on a 3D-2D modelling method, and estimate the cortical thickness using thresholding and morphological operations. Thresholding techniques, however, have been shown to be less accurate when estimating thin cortices [30]. Humbert *et al*. [31] propose a method to assess the cortex and trabecular macrostructure of the proximal femur in 3D from an AP DXA

scan. A model-based approach is used to estimate the cortical thickness and density [32], providing accurate measurements even for thin cortices.

Applying such methodologies to obtain 3D subject-specific shape and density estimation of the lumbar spine from DXA scans is not straightforward: DXA spine images are much noisier than hip DXA scans because rays have more biological tissue to penetrate; geometry of the spine is more complex than the one of the femur; and the presence of more than one anatomical structure (i.e. 4 lumbar vertebrae) requires modelling inter-object relationships besides shape and density. Moreover, the cortex of the vertebral body is very thin (from 180 to 600 µm with a mean thickness of 380 µm [33], [34]), which makes the segmentation of the cortical and trabecular bone very challenging. Whitmarsh *et al*. [35] obtain 3D subject-specific estimates of the lumbar spine (from L2 to L4) using two DXA images (AP and lateral views). For each vertebra, a statistical shape and density model is generated. The three models are simultaneously registered onto the AP and lateral DXA scans to generate a 3D model of the lumbar spine. Although measurements are performed in the trabecular compartment, no specific algorithm is proposed to quantify the cortical bone. Furthermore, lateral spine imaging with densitometric Vertebral Fracture Assessment (VFA) is used in clinical practices to evaluate the presence of vertebral fractures. However, VFA (which uses single-energy X-rays) does not measure BMD. Due to high precision errors, lateral DXA (i.e. double-energy) scans should not be used for osteoporosis screening [8]. To the best of our knowledge, no 3D modelling methods of the shape and density of the lumbar spine, or its cortical and trabecular bone assessment, using a single AP DXA scan, has been reported in the literature.

In this paper, we propose a method to estimate the shape and vBMD at the lumbar spine (from vertebra L1 to L4) using a single AP DXA image. The method is based on a 3D statistical shape and density model built from a training set of 90 QCT scans. The model describes the principal statistical variations in shape and density observed in the training database. A 3D shape and density estimation of the lumbar spine is obtained by registering and fitting the statistical model onto the AP DXA image. Then, a model-based algorithm is used to segment the cortical layer and propose a separate assessment of the trabecular and cortical bone at the vertebral body. Clinical measurements are performed at different vertebral regions and bone compartments. Finally, the accuracy of the method is evaluated by comparing DXA-derived with QCT-derived 3D subject-specific models and clinical measurements for a validation set of 180 subjects.

II. MATERIALS AND METHODS

A. Study subjects and medical images

Two different databases collected by the CETIR Centre Mèdic (Barcelona, Spain) were used in this study: a training database (90 subjects) to generate the statistical shape and density model (Section II.B), and a validation database (180 subjects) to evaluate the accuracy of the DXA-derived 3D

measurements (Section II.E).

Subjects included in both databases were adult men and women. Exclusion criteria included skeletal disease other than osteoporosis, such as severe osteoarthritis, severe scoliosis or abnormal bone growth and vertebral fracture. An additional criterion to recruit the subjects included in the validation database was to obtain the same number of subjects in each category used to define bone density: 30 subjects with osteoporosis, 30 with osteopenia and 30 with normal bone density; with a 2/3 female and 1/3 male ratio.

All subjects included in the training and validation database presented clinical indications for an AP DXA scan at the lumbar spine. When DXA scan confirmed that inclusion/exclusion criteria were met, the subjects were invited to participate to the study and abdominal QCT scans were performed. AP DXA and QCT scans were therefore performed for all participants. Both scans were analyzed and interpreted by radiologists. AP DXA scans of the training set were used to ensure inclusion/exclusion criteria were met; whereas AP DXA scans of the validation set were also used to generate the 3D subject-specific estimations. QCT scans of the training set were used to generate the statistical shape and density model; whereas QCT scans of the validation set were used as ground truth to evaluate the accuracy of the estimated DXA-derived 3D measurements. Volunteers were informed about the purpose of the study, the potential risks of undergoing explorations in which they would be subjected to ionizing radiations and the subsequent use of their anonymized scans. Volunteers were recruited until achieving the desired number of subjects in each group. The study was approved by the Committee of Clinical Investigation of "Fundació d'unió Catalana d'hospitals" and written informed consent was obtained from all subjects. Subjects included in the training and validation sets were collected prospectively within the European Eurostars Project (ID: 9 140).

The AP DXA scans were performed at CETIR Centre Mèdic using a Lunar iDXA scanner (GE Healthcare, Madison, WI) or a Stratos dR DXA scanner (DMS, Mauguio, France). aBMD at vertebrae L1 to L4 (L1-L4 segment) was measured in the DXA images and T-score was computed using the enCORE software (GE Healthcare) or Stratos software (DMS), respectively. Participants were categorized using the T-score of the L1-L4 segment, following the ISCD recommendations [8], as: normal bone mass or healthy (T-score $\geq$ -1), low bone mass or osteopenia (-2.5 < T-score < -1) or osteoporosis (T-score $\leq$ -2.5). Vertebrae affected by local structural changes or artefacts were excluded to derive the T-score. However, this criterion was not used as exclusion criteria for the subject, neither to discard vertebrae for the statistical model generation nor for the 3D estimation.

The QCT scans were performed at the lumbar spine, in a region of interest including at least vertebrae L1 to L4. The study subjects were scanned at CETIR Esplugues PET (Esplugues de Llobregat, Spain) using a Philips Gemini GXL 16 (Philips Healthcare, Best, The Netherlands) or a GE HiSpeed QX/I scanner (GE Healthcare), and at CETIR Clinica del Pilar (Barcelona, Spain) using a GE Discovery CT750 HD

scanner (GE Healthcare). The QCT voxel size ranged from 0.64 mm × 0.64 mm × 0.5 mm to 1.10 mm × 1.10 mm × 0.5 mm (average pixel size: 0.86 mm × 0.86 mm), with a matrix size of 512 × 512 pixels. The scans were acquired with a distance between consecutive slices of 0.5 mm, slice thickness ranging from 1 to 1.25 mm, convolution kernel A (Philips scanner) and standard (GE scanners), x-ray source potential of 120 kVp, tube current ranging from 138 to 188 mA, resulting in a dose index (CTDIvol) ranging from 10.0 to 11.6 mGy. A calibration phantom (Mindways Software Inc., Austin, TX) was scanned together with the subjects.

Three subjects of the validation set were selected as examples for some of the figures presented in this paper: a healthy female (T-score of 1.1), a female with osteopenia (T-score of -2) and a female with osteoporosis (T-score of -3.9)[1].

B. Statistical shape and density model generation

A statistical shape and density model was built using the 90 QCT scans collected from the training database as follows.

1) Data pre-processing

DICOM images from QCT scans were converted in volumetric images (i.e. 3-dimensional matrices where each element is a sampled density) and calibrated using the Mindways phantom. The calibration process was performed for each L1-L4 segment, for the 90 subjects in the training set, following the protocol recommended by the manufacturer.

The calibrated QCT volumes were filtered to enhance the contrast in the facet joints, thereby helping the individual segmentation of each vertebra [36], as follows. First, small groups of bright voxels at vertebral joint space were darkened using a 3D opening filter. Then, a top-hat filter was applied to highlight the brightest areas (vertebral bone); and a bottom-hat filter was applied to highlight the darkest areas (facet joints). Finally, the contrast between bone and facet joints was enhanced adding to the QCT volume the top-hat filtered volume and subtracting the bottom-hat filtered volume. The filtered QCT volumes were used only to help segmentation, not to generate the statistical density model.

Vertebrae were semi-automatically segmented in the pre-processed QCT volumes using the software TurtleSeg [37], [38], which implements the following process. The vertebral contours are manually identified in a set of non-parallel slices. The software automatically interpolates the contours to form a 3D segmentation, resulting in a volumetric mask for each vertebra. If the results are not satisfactory, additional contours are identified and the interpolation is repeated. Local deformities, such as spurs, were manually segmented by painting and erasing techniques. The segmentation process was performed for each vertebra, and for the 90 subjects in the training set. The segmentation process took between forty minutes and two hours to segment each vertebra of the L1-L4 segment, depending on the image quality and the presence of local deformities of the vertebrae.

---

[1] The AP DXA and QCT images obtained for these subjects with close ups on the L2 vertebra are provided as supplementary downloadable material (Appendix A) in the supplementary files /multimedia tab.

Finally, the resulting 3D vertebral masks are subsampled and smoothed with a Gaussian filter. A triangulated surface mesh between 5638 and 15368 vertices and between 11276 and 30772 faces is generated for each vertebra[2].

2) Shape alignment

The surface meshes resulting from the segmentation process have different number and arrangement of vertices and faces. Point set registration techniques are used at each vertebral level (L1, L2, L3 and L4) to create correspondence between the vertices of the surface meshes. First, a lumbar spine having a normal aBMD (T-score ≥ -1) and without local deformities, such as bone spurs, is chosen among the subjects of the training set. The vertebrae L1 to L4 of the chosen lumbar spine are used as reference for its respective vertebral level. Then, the vertices of the reference mesh are non-rigidly registered onto the vertices of each surface mesh of the training set using the Coherent Point Drift (CPD) algorithm. Details of CPD algorithm can be found elsewhere [39], [40].

To improve the accuracy of the meshes resulting from the CPD registration process, each surface mesh is projected onto its corresponding original surface mesh using the normal vectors of the vertices of the meshes. This sometimes results in meshes including flipped faces, which are detected by comparing the orientation of the normal vectors to the faces of the meshes after and before projection. Flipped faces are then corrected by replacing the projected vertices by its nearest point on the original surface mesh, and by smoothing the neighboring region. Projection of the mesh vertices and flipped faces detection/correction algorithm is repeated iteratively until no flipped face is detected. This results in a set of surface meshes having the same number and arrangement of vertices and faces within each vertebral level (4545, 5025, 5437 and 5421 vertices and 9090, 10050, 10874 and 10842 faces for L1, L2, L3 and L4, respectively). The accuracy of the point set registration process was evaluated by computing the signed distance between each vertex of registered reference mesh and its nearest point in the original surface mesh. At the end of the process, the mean distance (± SD) computed for all vertebrae of the training database was -0.0017 ± 0.0765 mm, with a maximum distance of 1 mm.

Finally, the surface meshes of the L1-L4 segment obtained for the 90 subjects are aligned (scaled, rotated and translated) using Generalized Procrustes Analysis (GPA) [41].

The above-described registration process is biased by the choice of the reference shape that is used at the beginning of the process. The shape alignment process is thus iterated to correct for this bias. At each iteration it, the reference mesh is replaced by the average shape of the surface meshes obtained at the end of iteration $it - 1$ (i.e. after GPA alignment). The point-to-surface distances between the reference shapes at iterations it and $it - 1$ are computed to study the convergence of the process. The process converged after five iterations.

---

[2] Details and images showing the segmentation process are provided as supplementary downloadable material (Appendix B) in the supplementary files / multimedia tab.

3) Statistical shape model

The SSM of the lumbar spine is defined as the mean position of the vertices and the main modes of variation describing the linear displacements of the vertices from their mean position [42]. Each ith lumbar spine (L1-L4 segment) obtained after the shape alignment process is represented by a $3n$ element vector $\boldsymbol{s}_i = (\boldsymbol{x}_1, \boldsymbol{x}_2, \ldots \boldsymbol{x}_n)^T$ with $\boldsymbol{x} = [x, y, z]$ gathering the position of its n vertices. Principal Component Analysis (PCA) [43] is used to reduce the space dimensionality, assuming all lumbar spine shapes in the training dataset follow a Gaussian distribution. The mean $\bar{\boldsymbol{s}}$ and covariance $\boldsymbol{\Sigma}$ of the point cloud take the form:

$$\bar{\boldsymbol{s}} = \frac{1}{k} \sum_{i=1}^{k} \boldsymbol{s}_i \tag{1}$$

$$\boldsymbol{\Sigma} = \frac{1}{k-1} \sum_{i=1}^{k} (\boldsymbol{s}_i - \bar{\boldsymbol{s}})(\boldsymbol{s}_i - \bar{\boldsymbol{s}})^T \tag{2}$$

where k is the number of training shapes. Eigenvectors $\boldsymbol{\rho}_j$ and eigenvalues λ_j with $j = 1, \ldots, k - 1$ of the covariance matrix $\boldsymbol{\Sigma}$ are computed as described by Cootes *et al.* [44]. The eigenvectors $\boldsymbol{\rho}_j$ represent the principal modes of variation, and the eigenvalues λ_j represent the variance of the data around the mean in the direction of the corresponding eigenvector $\boldsymbol{\rho}_j$. Lumbar spine shapes in the PCA domain can be expressed as:

$$\boldsymbol{s} = \bar{\boldsymbol{s}} + \boldsymbol{P}\boldsymbol{a} \tag{3}$$

where $\boldsymbol{P} = (\boldsymbol{\rho}_1 \boldsymbol{\rho}_2 \ldots \boldsymbol{\rho}_p)$ is the matrix of the principal components (the first p modes of variation, corresponding to the most significant eigenvectors) and $\boldsymbol{a}$ is a p-dimensional vector of scalar coefficients weighting the contribution of each principal component.

The range of variation of the shape parameters $\boldsymbol{a}$ is bounded to avoid that implausible lumbar spine shapes are modelled. After examining the distribution of the $\boldsymbol{a}$ values required to generate the shapes of the training set [44], we choose to approximate the shape space domain (subspace of allowed shapes) by a hyperrectangular space, applying hard limits of ± 3 times the standard deviations along each principal component:

$$|a_j| < 3\sqrt{\lambda_j} \tag{4}$$

4) Volume alignment

The calibrated QCT volumes at the L1-L4 segment are aligned to remove the shape variability and to assure that the statistical density model captures only variations related to density. Thin Plate Spline (TPS) transformations [45] are computed between the mean SSM ($\bar{\boldsymbol{s}}$) of the L1-L4 segment and each one of the spine shapes obtained before GPA alignment (and after the correspondence of the vertices), Fig. 1a. 8000 vertices (resulting from the decimation of the mean shape) are used as control points to compute the TPS transformations. The accuracy of the TPS transformations was

evaluated by applying the transformations to the mean shape $\bar{s}$ and computing the signed distance between each vertex of the transformed shape and its nearest point in the surface mesh obtained before GPA alignment. The mean distance (± SD) computed for all spine shapes of the training database was 0.00023 ± 0.14830 mm.

A volumetric grid initialized over $\bar{s}$ is used as template for sampling. The grid size is set up so that it encompasses the mean L1-L4 segment shape plus 15 mm in each direction, with a voxel size of 1 mm^3. The reference volumetric grid is filled with null values. The computed TPS transformations are applied to the reference grid to obtain 3D displacement fields, Fig. 1b. Density values at the deformed grid coordinates are computed by tri-linear interpolation in the original calibrated QCT volumes. The computed density values are used to fill the reference 3D template, Fig. 1c. This results in a set of volumetric images with the size and resolution of the 3D reference template, and the shape of the mean SSM, however maintaining their original density content.

5) Statistical density model

The statistical density model of the lumbar spine is defined as the mean density values, each one corresponding to a voxel in the reference 3D template image, and the main modes of variation describing the density distribution from their mean value. A binary mask is generated over the mean SSM ($\bar{s}$) and applied to the aligned volumetric density images to capture only the density variations inside the 4 lumbar vertebrae. Each lumbar spine obtained after the volume alignment process is represented by an m element vector $\mathbf{g}_i = (d_1, d_2, \ldots, d_m)^T$ gathering the bone density values contained in the m voxels inside the binary mask. PCA is used to extract principal density variation modes using the computed density matrix as inputs. New density volumes are defined as:

$$\boldsymbol{g} = \bar{\boldsymbol{g}} + \boldsymbol{Qb} \tag{5}$$

where $\bar{\mathbf{g}}$ is the mean density volume of the training set, $\boldsymbol{Q} = (\boldsymbol{\rho_1}\boldsymbol{\rho_2}\ldots\boldsymbol{\rho_q})$ is the matrix of the principal components (the first q modes of variation) and $\boldsymbol{b}$ is a q-dimensional vector of scalar coefficients weighting the contribution of each principal component. The parameters are calculated as in Section II.B.3). Density parameters $\boldsymbol{b}$ are constrained as in (4).

6) Model instance

The statistical shape and density model built is composed by a mean shape and density volume, and a set of components modelling the principal variations observed in the training set[3]. An instance of the statistical model is generated as follows.

Starting from the mean density $\bar{\boldsymbol{g}}$ and the mean shape $\bar{\boldsymbol{s}}$ of the statistical model, a temporary density instance $\boldsymbol{g}$ is generated, using (5), over the mean shape $\bar{\boldsymbol{s}}$, Fig. 2a. Then, a shape instance $\mathbf{s}$ is generated by deforming the mean shape $\bar{\boldsymbol{s}}$ using (3) and by subsequently applying a similarity transform $\boldsymbol{T}$:

[3]The statistical model variations in the three principal directions, can be seen in a video graphical abstract available in the supplementary files /multimedia tab.
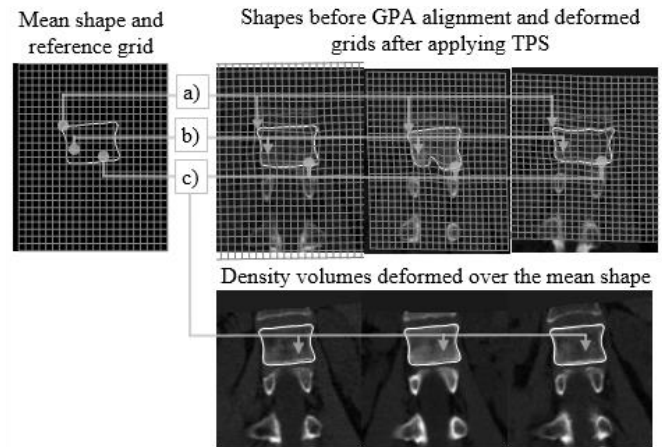

Fig. 1. Lumbar spine volume alignment: a) Compute TPS transformations between the mean shape and surface shapes; b) Apply TPS transformations to the reference volumetric grid; c) Interpolate and assign density values to the reference grid. The alignment process is applied to the four vertebrae simultaneously (L1-L4 segment); in this figure, only one vertebra is shown for better visualization.
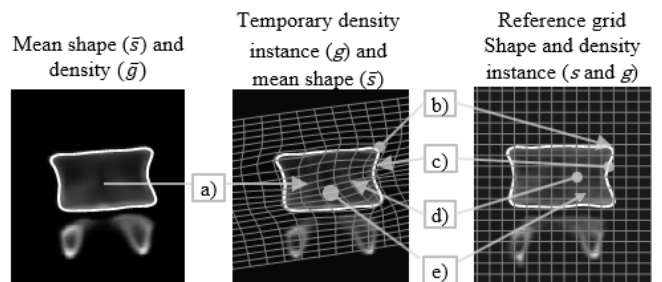

Fig. 2. Model instance generation a) Generate density instance; b) Generate shape instance; c) Compute TPS transformation; d) Apply TPS transformation; e) Interpolate. The model instance is generated for the four vertebrae simultaneously (L1-L4 segment); in this figure, only one vertebra is shown for better visualization.

$$\boldsymbol{T}(s) = \alpha \boldsymbol{R} s + \boldsymbol{t} \tag{6}$$

where α is the scaling, $\boldsymbol{R}$ the 3x3 rotation matrix determined by the rotation angles $(\theta_x, \theta_y, \theta_z)$ around $(\vec{x}, \vec{y}, \vec{z})$ axes and $\mathbf{t} = (t_x, t_y, t_z)^T$ the translation vector, Fig. 2b. Then, the temporary density instance $\boldsymbol{g}$ is deformed onto the shape instance $\mathbf{s}$ as follows. A TPS transformation between the shape instance $\mathbf{s}$ and the mean shape $\bar{\boldsymbol{s}}$ is computed using 1000 vertices as control points, Fig. 2c. The control points are obtained by decimation of the original shapes. A reference volumetric grid is created over the shape instance $\mathbf{s}$ and the calculated TPS transformation is applied to the reference grid, Fig. 2d. The density values at the transformed grid are interpolated in the temporary density instance. Finally, the reference volumetric grid is filled using the interpolated density values, Fig. 2e.

C. 3D subject-specific shape and density estimation from DXA images

A 3D subject-specific shape and density lumbar spine estimation is obtained by performing a 3D-2D registration of the statistical shape and density model onto the AP DXA scan of the patient, Fig. 3. The AP DXA scans from the validation database are used to generate the DXA-derived 3D subject-specific estimations.

1) 2D Mask

A 2D binary mask is automatically generated over the lumbar spine region to define the region of interest of the DXA image to be used in the 3D-2D registration process. A mask over the bony structures and a set of landmarks that defines a quadrilateral over each vertebra, both provided by the DXA scanner manufacturer software, are used. The mask over the bony structures is cropped over L1 and below L4, using the landmarks associated with these two vertebrae, Fig. 3 ("Bone Mask" image). Then, the resulting mask is slightly dilated in the lateral direction using a disk-shaped structural element (radius 8), Fig. 3 ("L1-L4 Mask" image).

2) 3D-2D Registration

The 3D-2D registration is an iterative process of registration and fitting based on a 3D-2D intensity-based registration method[4]. At each iteration, an instance of the 3D model is created, and a 2D image is generated using a parallel projection of the 3D model in the AP direction, Fig. 3 ("Model Instance" and "2D Projection" images). Current narrow-angle fan beam DXA scanners, such as Lunar iDXA (GE) and Stratos dR DXA (DMS), generate AP DXA images essentially without magnification. Therefore, the density of the model instance I_{Model} is projected, using a parallel projection in the $\vec{z}$ direction, to generate the simulated 2D image I_{Sim}:

$$I_{\text{Sim}}(x, y) = \sum_z I_{Model}(x, y, z) \tag{7}$$

The following model instance parameters are optimized to maximize the similarity between the projection of the model instance I_{Sim} and the DXA image I_{DXA}: the pose parameters $(\alpha, \theta_x, \theta_y, \theta_z, t_x, t_y)$, the shape model parameters $\boldsymbol{a}$ and the density model parameters $\boldsymbol{b}$. The translation in the $\vec{z}$ direction is not optimized because the model is projected in that direction.

The similarity between I_{Sim} and I_{DXA} is measured in the 2D binary mask region of interest as:

$$E(\alpha, \boldsymbol{\theta}, \boldsymbol{t}, \boldsymbol{a}, \boldsymbol{b}) = \frac{1}{P} \sum_{v \in Mask} (I_{Sim}(v) - I_{DXA}(v))^2 \tag{8}$$

where P is the number of pixels set to 1 in the mask. The parameters of the model are optimized in a 3-step process using Powell's conjugate direction method [46]. In the first step, translation and scale parameters are optimized. In the second step, the rotation is optimized in addition to the translation and scale parameters. In the third step, a non-rigid registration is performed and all parameters are optimized. Each step is iterated until the cost function values at the current parameter and at the local extrema are within a tolerance of 0.01.

3) Model initialization

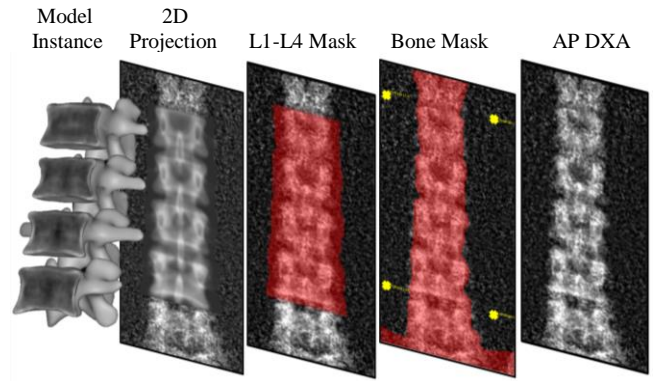The model is initialized as follows. The scale is set to 1 and

---

Fig. 3. 3D-2D registration process. Left to right: instance of the statistical shape and density model, parallel projection of the 3D model in the AP direction, 2D mask over the L1-L4 segment, mask over bony structures and landmarks, and AP DXA image.

the rotation angles to 0. The initial translation is set up to align the center of the model with the center of the 2D mask (Fig. 3, "L1-L4 Mask" image). The mean density and shape instance of the statistical model is used in the first iteration (shape and density parameters $\boldsymbol{a}$ and $\boldsymbol{b}$ set to 0). Shape and density model parameters $\boldsymbol{a}$ and $\boldsymbol{b}$ are bounded by (4), thereby guaranteeing new model instances deform into lumbar spines conforming to global constraints imposed by the training set. The accurate model initialization obtained using the L1-L4 mask (Fig. 3) and the coarse-to-fine registration described in Section II.C.2) helps the convergence of the optimization process.

D. Geometrical and bone mineral density measurements

1) Periosteal and endocortical shapes

The cortical layer is segmented in the density volumes resulting from the 3D-2D registration process to perform a separate assessment of the cortical and trabecular bone. The periosteal (outer) and endocortical (inner) surfaces of the cortical layer are found by adapting the model-based algorithm described in Humbert *et al.* [32] as described below and illustrated in Fig. 4. At each vertex of the shape model instance **s**, the density profile along the normal vector to the vertebral surface is measured by linearly interpolating in the density volume **g** (black line in Fig. 4). The profile extends 2 mm outside the vertebral surface shape and 4 mm inside. The modelled density profile (grey line in Fig. 4) is described as:

$$d_{mod}(\boldsymbol{x}) = d_0 + \frac{d_1 - d_0}{2} \left(1 + \text{erf}\left(\frac{x - \left(x_1 - \frac{\Delta}{2}\right)}{\sigma\sqrt{2}} \right) \right) + \frac{d_2 - d_1}{2} \left(1 + \text{erf}\left(\frac{x - \left(x_1 + \frac{\Delta}{2}\right)}{\sigma\sqrt{2}} \right) \right) \tag{9}$$

where d_0, d_1 and d_2 represent the density values in the surrounding tissue, within the cortex and within the trabeculae, respectively; $\boldsymbol{x}_1$ the central position of the cortical shell; Δ is the cortical thickness; and σ is the standard deviation of the blur caused for the response of the imaging system and modelled as a normalized Gaussian function.

The position of the outer and inner surfaces of the cortical layer are determined by searching the optimal values of the cortical thickness Δ and the center position of the cortical shell

---

[4] The 3D-2D registration process can be seen in a video graphical abstract available in the supplementary files /multimedia tab.

x_1, so that the modelled density matches the measured density profile. The Levenberg-Marquardt algorithm is used to find the optimal values. Fig. 4 shows a density model instance with line crossing the cortex shell where the density profile is measured. The measured density profile across the line is represented by the black dashed line.

In the optimization the model is constrained using prior information about the relationship between the cortical thickness Δ and the cortical density d_1, in the form of a look-up table, thus eliminating d_1 from the optimization. The periosteal and endocortical surfaces are only estimated at the vertebral body[5]. The interior of the endocortical shape defines the trabecular compartment, and the volume between the periosteal and endocortical shapes the cortical one. The integral bone is the union of the cortical and trabecular bone compartments.

2) Clinical measurements

Geometry and density measurements are provided for clinical practice purposes. Volume, BMC and vBMD are measured at the integral bone of the total vertebra and vertebral body. These measurements are also obtained for the trabecular and cortical compartments individually at the vertebral body. The cortical thickness is obtained by measuring the distance between the periosteal and endocortical surfaces. The mean cortical thickness at the vertebral body (CTh) is provided. Besides individual measurements for each vertebral level, measurements of the L1-L4 segment are also provided. In total, 65 features are measured for each subject. Finally, a surface map of the cortical thickness distribution of each vertebra is generated.

E. Validation method

The developed method was validated by comparing DXA-derived with QCT-derived 3D subject-specific shape and density estimates and clinical measurements using the validation set (180 subjects). The DXA and QCT-derived shape and density obtained for the three subjects selected as examples are shown in Fig. 5.

3D subject-specific shape and density estimations (Fig. 5 2nd column) were generated from the AP DXA scans of the validation set (Fig. 5 1st column) by using the methodology proposed in Section II.C. Two surfaces delimiting the cortical shell (periosteal and endocortical surfaces) at the vertebral bodies were estimated, and the cortical thickness and density were measured at each vertex of the surface meshes as described in Section II.D.1). The clinical measurements were computed as described in Section II.D.2).

On the other hand, QCT scans from the validation set were calibrated and segmented using the method described in Section II.B.1) (Fig. 5 3rd column). Position and curvature of the L1-L4 segments slightly differed between QCT and DXA acquisitions. For comparison purposes, each DXA-derived vertebral surface was aligned with its corresponding QCT-derived surface using rigid transformations (Fig. 5 4th

[5] The cortex analysis can be seen in a video graphical abstract available in the supplementary files /multimedia tab.
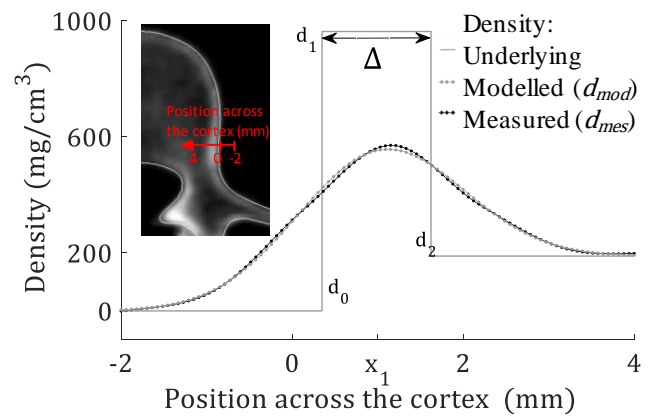

Fig. 4.   (Left) Shape and density model instance (axial view) with red line crossing the cortex shell where the density profile is measured. (Right) Density profile measured along the red line (d_{mes}) and modelled density (d_{mod}) resulting from the Gaussian blur applied to the underlying density variations. d_0, d_1, d_2 are the density values in the surrounding tissue, within the cortex, and within the trabecular bone, respectively; Δ is the cortical thickness, and x_1 the location of the center of the cortex.

column). Rigid alignments were performed using the CPD algorithm [39], [40]. The region corresponding to the vertebral body of each aligned DXA-derived mesh was projected onto its corresponding QCT-derived mesh. The resulting vertebral body regions of interest, defined over the QCT surfaces, were used to estimate the cortical shell (using the model-based approach described in Section II.D.1) and to compute the clinical measurements (Section II.D.2).

At each vertebral level, shape accuracy was measured using the point-to-surface distances between the vertices of the aligned DXA-derived and their corresponding QCT-derived periosteal surfaces. The cortical thickness and density distributions obtained with the two modalities were compared. The linear correlations between DXA and QCT-derived measurements were evaluated using the Pearson's correlation coefficient. The statistical significance of the differences between measurements was evaluated using the Student's t-test. The experiments were done using an IntelCore i7-4790K CPU 3.60 GHz, 4 cores (8 treads), 64-bit, 16 GB of RAM with Windows 10.

III. RESULTS

The training set was formed by 90 subjects (66 females and 24 males) with a mean age of 55.2 ± 11.3 years and a range between 30 and 83 years. The set was composed by 36 subjects with normal bone mass, 37 with low bone mass and 17 with osteoporosis. Mean T-score was -1.29 ± 1.31 with a range between -3.5 and 2.4.

The validation set was formed by 180 participants. 90 subjects (60 females and 30 males) with a mean age of 59.1 ± 10.5 years and a range between 28 and 84 years were scanned using the Lunar iDXA device. 90 other subjects (60 females and 30 males) with a mean age of 54.1 ± 12.3 years and a range between 22 and 84 years were scanned using the Stratos dR device. Mean T-score was -1.26 ± 1.83 with a range between -4.4 and 3.4.
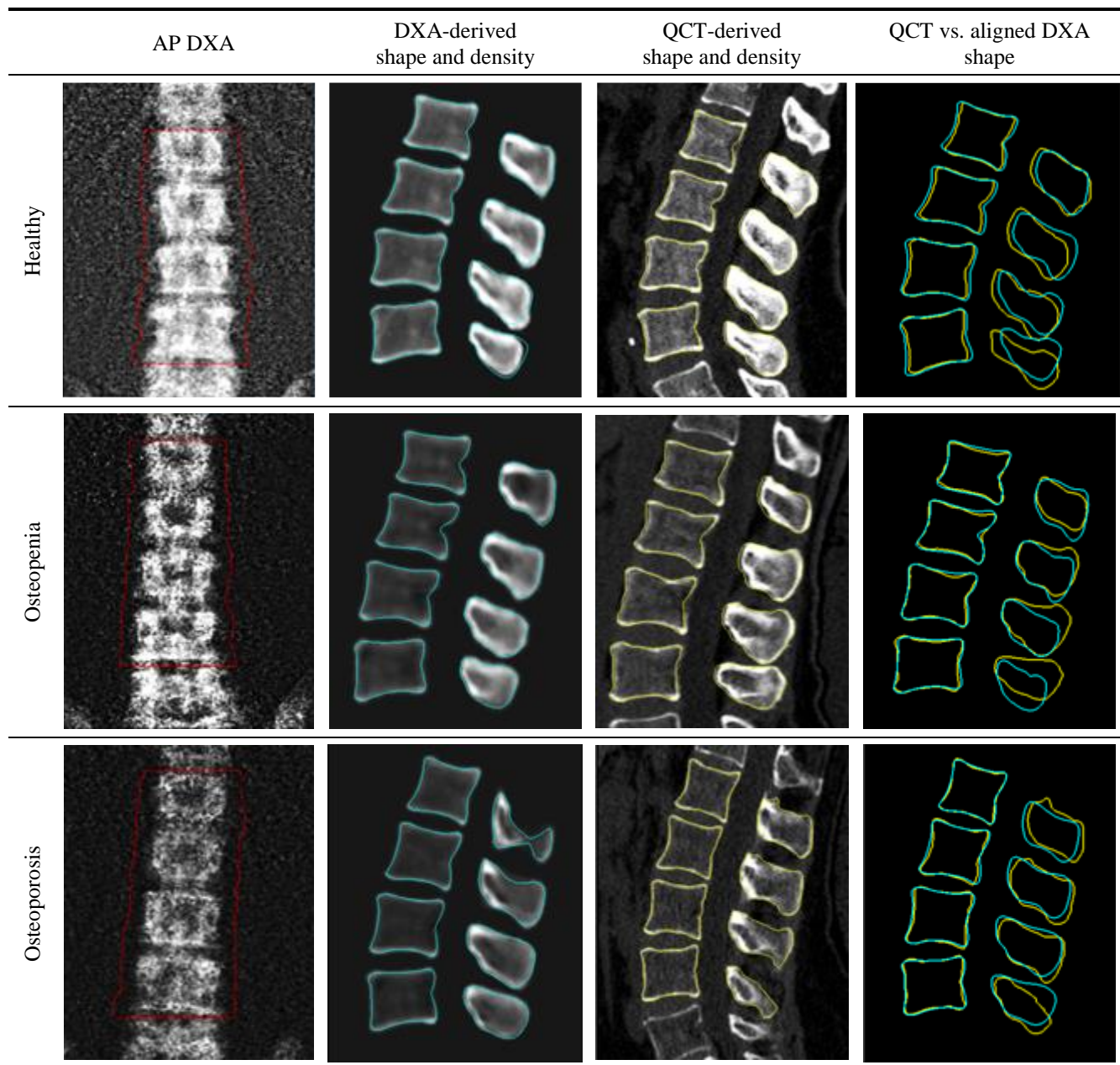
Fig. 5.   Comparison of the DXA-derived and QCT-derived 3D subject-specific shape and density of the lumbar spine for three subjects selected as examples. 1st column: AP DXA image with its 2D mask over the L1-L4 segment. 2nd column: Frontal slice of the 3D subject-specific shape and density estimated from the AP DXA image. 3rd column: Frontal slice of the QCT density and segmented shape. 4th column: QCT segmented shape and DXA-derived shape rigidly aligned onto the QCT shape.

A. Shape accuracy

Shape accuracy was measured at each vertebral level as described in Section II.E. Average point-to-surface distance between subject-specific periosteal surfaces obtained by DXA and QCT was 1.51 mm for the L1-L4 segments (Table I). A shape accuracy of 0.66 mm was achieved at the vertebral body. Similar point-to-surface distances were obtained for different vertebrae (L1 to L4) and datasets (using GE and DMS scanner). The systematic error (or bias) for the total vertebra shape was low (-0.05 mm for the L1-L4 segment), however significant (p-value < 0.01). The systematic error at the vertebral body was slightly higher (0.13 mm for the L1-L4 segment, p-value < 0.01). The random error was lower for the

vertebral body (SD of 0.84 mm), compared to total vertebra (SD of 2.02 mm), due to larger errors in modelling the back process.

B. Cortical thickness and density distribution

DXA-derived and QCT-derived cortical thickness and density were compared. An average difference of -0.01 ± 0.14 mm and a mean absolute error of 0.10 mm were found for the cortical thickness in the L1-L4 segment. An average difference of -4.07 ± 74.49 mg/cm^3 and a mean absolute error of 47.00 mg/cm^3 was measured for the cortical density. The systematic error for the cortical thickness and density were low, however significant (p-value < 0.01). Differences for

each vertebral level and each dataset were similar[6].

The DXA and QCT-derived cortical thickness distribution obtained for the three example subjects are shown in Fig. 6. Cortical thicknesses follow a similar distribution between each pair, although the DXA-derived cortical thickness tends to be slightly thinner than the QCT-derived. The figure also shows that the healthy subject has a higher cortical thickness, compared to the subject with osteopenia and osteoporosis.

C. Clinical measurements

DXA and QCT-derived clinical measurements for the L1-L4 segment were compared, Table II. A correlation coefficient (R) of 0.91 was found between DXA and QCT-derived integral vBMD at the total vertebra, and of 0.85 at the vertebral body (whole database). The R-values ranged from 0.81 to 0.97, depending on the clinical measurements and datasets used. R-values obtained for vBMD and BMC in the cortical layer were slightly higher than the ones found for the trabecular compartment. Using the whole database of subjects, the integral vBMD of total vertebra was on average higher when estimated by DXA, compared to QCT (4.63 ± 23.82 mg/cm^3), although this difference was not significant. A statistically significant difference between DXA and QCT-derived measurements was found for the trabecular vBMD and BMC at the vertebral body (p < 0.01), when the whole database is compared[7].

The mean computing time to generate the DXA-derived 3D subject-specific models and clinical measurements was 3 min 28 s and ranged between 2 min 38 s and 5 min 31 s.

IV. DISCUSSION

In this paper, we introduced a method to estimate the 3D shape and vBMD distribution of the lumbar spine (L1-L4 segment) from a single AP DXA image, and to assess the cortical and trabecular bone. The method proposed is fully automated: no user iteration is needed[8]. Most of state-of-the-art 3D modelling methods require a set of landmarks to be positioned in the DXA image, [28], [29], [35].

An IntelCore i7-4790K CPU 3.60 GHz was used to process the AP DXA scans and obtained the 3D subject-specific models. The mean (±SD) number of iterations was 1628 ± 218, achieving a mean computing time of 3 min 28 s. The computing time mostly depended on the size of the region of interest used in the 3D-2D registration process (L1-L4 mask, Fig. 3). The larger or wider the L1-L4 segment, the higher the computing time. Low computation time is one of the requirements of clinical practice. Humbert *et al*. [31] achieved the lowest computing time for the femur (1 min 30 s using an

Table I.
Point-to-surface distances (mm) between the aligned periosteal surfaces of the 3D subject-specific shapes estimated by DXA and QCT: Mean ± Standard Deviation (SD) of the signed distances and mean of the unsigned (uns.) distances. Region of interest: vertebral shape ("Total") and vertebral body ("Body").

		All (N =180)		GE (N =90)		DMS (N =90)	
		Mean ± SD	Mean (uns.)	Mean ± SD	Mean (uns.)	Mean ± SD	Mean (uns.)
L1	Total	0.02 ± 1.80*	1.37	0.02 ± 1.82*	1.39	0.03 ± 1.78*	1.36
	Body	0.22 ± 0.85*	0.68	0.20 ± 0.86*	0.68	0.25 ± 0.85*	0.68
L2	Total	-0.03 ± 1.82*	1.39	-0.03 ± 1.83*	1.39	-0.04 ± 1.81*	1.38
	Body	0.17 ± 0.83*	0.65	0.16 ± 0.84*	0.66	0.18 ± 0.83*	0.65
L3	Total	-0.06 ± 4.05*	1.53	-0.09 ± 2.03*	1.52	-0.04 ± 2.06*	1.53
	Body	0.09 ± 0.82*	0.63	0.06 ± 0.81*	0.63	0.13 ± 0.83*	0.64
L4	Total	-0.10 ± 2.35*	1.72	-0.15 ± 2.34*	1.71	-0.05 ± 2.35*	1.73
	Body	0.06 ± 0.86*	0.67	0.02 ± 0.86*	0.68	0.10 ± 0.86*	0.67
L1-L4 segment	Total	-0.05 ± 2.02*	1.51	-0.06 ± 2.02*	1.51	-0.03 ± 2.0*	1.51
	Body	0.13 ± 0.84*	0.66	0.11 ± 0.85*	0.66	0.16 ± 0.93*	0.66

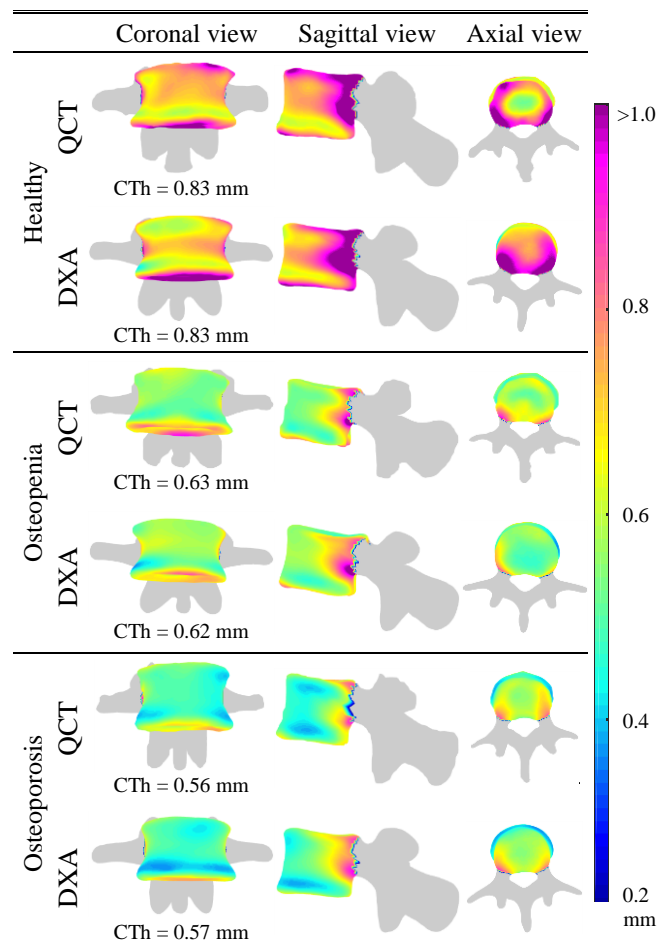* p-value < 0.01, Student's Test

Fig. 6. Comparison of DXA-derived and QCT-derived cortical thickness distribution for the three subjects selected as examples.

IntelCore i7-4790K CPU 4.0 GHz), in comparison with Väänänen *et al*. [29] (40 hours using an Intel Sandy Bridge 2.6 GHz) or Whitmarsh *et al*. [28] (1 hour using an IntelCore i7 CPU 920 2.67 GHz). The method developed by Whitmarsh *et al*. [35] took more than 4 h (using an IntelCore i7 CPU 920

---

[6] Details are provided in Appendix C (supplementary files/multimedia tab).

[7] DXA and QCT-derived clinical measurements and their comparison for each vertebral level (i.e. L1, L2, L3 and L4); and a comparison of the measurements for each category used to define bone density (healthy, osteopenia and osteoporosis) are provided in Appendix D. The DXA-derived vBMD value was plotted against its corresponding QCT-derived vBMD measure for each subject of the DMS validation set, Appendix E (supplementary files /multimedia tab).

[8] The workflow of the proposed method can be seen in a video abstract available in the supplementary files / multimedia tab.

Table II.

Values (mean ± standard deviation) and differences (mean ± standard deviation) between DXA-derived and QCT-derived clinical measurements: Values and correlation coefficients R are provided for the total vertebra ("Total") and vertebral bodies ("Body").

L1 – L4 Segment			All (N = 180)				GE (N = 90)		DMS (N = 90)	
			QCT	DXA	Difference (DXA - QCT)		Difference (DXA - QCT)		Difference (DXA - QCT)	
			Mean ± SD	Mean ± SD	Mean ± SD	R**	Mean ± SD	R**	Mean ± SD	R**
vBMD (mg/cm³)	Integral	Total	281.65 ± 55.38	286.28 ± 57.31	4.63 ± 23.82	0.91	11.32 ± 23.73	0.91	-2.05 ± 22.08	0.93
		Body	212.61 ± 44.88	219.16 ± 43.32	6.55 ± 23.84	0.85	8.23 ± 24.36	0.83	4.87 ± 23.33	0.87
	Trabecular	Body	150.32 ± 40.35	161.57 ± 38.85	11.25 ± 23.31*	0.83	12.12 ± 23.30	0.81	10.37 ± 23.43	0.85
	Cortical	Body	611.18 ± 46.26	610.43 ± 40.77	-0.74 ± 25.14	0.84	0.82 ± 26.82	0.82	-2.30 ± 23.38	0.86
BMC (g)	Integral	Total	51.97 ± 13.90	52.46 ± 14.28	0.49 ± 4.29	0.95	1.49 ± 4.57	0.95	-0.51 ± 3.77	0.96
		Body	24.62 ± 6.79	25.86 ± 6.99	1.25 ± 2.82	0.92	1.31 ± 3.03	0.91	1.18 ± 2.61	0.93
	Trabecular	Body	15.04 ± 4.75	16.61 ± 4.95	1.56 ± 2.49*	0.87	1.54 ± 2.65	0.86	1.59 ± 2.35*	0.88
	Cortical	Body	9.58 ± 2.34	9.26 ± 2.20	-0.32 ± 0.88	0.93	-0.23 ± 0.92	0.93	-0.41 ± 0.84	0.93
Volume (cm³)	Integral	Total	184.80 ± 34.37	183.49 ± 33.78	-1.31 ± 9.33	0.96	-2.24 ± 9.65	0.96	-0.38 ± 8.95	0.97
		Body	116.17 ± 22.42	118.14 ± 21.83	1.97 ± 6.56	0.96	1.31 ± 6.48	0.96	2.63 ± 6.61	0.96
	Trabecular	Body	100.62 ± 20.12	103.08 ± 19.55	2.46 ± 6.34	0.95	1.69 ± 6.24	0.95	3.23 ± 6.39	0.95
	Cortical	Body	15.55 ± 2.92	15.05 ± 2.81	-0.49 ± 1.04	0.93	-0.38 ± 1.09	0.93	-0.60 ± 0.99	0.94
CTh (mm)	Cortical	Body	0.72 ± 0.08	0.71 ± 0.08	-0.02 ± 0.05	0.83	-0.01 ± 0.05	0.82	-0.03 ± 0.04	0.86

*p-value < 0.01, Student's Test

**R with p-value < 0.01 for all measurements.

2.67 GHz) to generate a 3D subject-specific estimation of the L2-L4 segment. We use C++, ITK and multi-core system techniques to achieve low computation times. Geometry of the spine is more complex than the one of the femur (our model had 20428 nodes, against 5546 for [31]; and four bone structures are assessed instead of one, which explains a higher computing time. This average computing time of less than 5 min, however, should be sufficiently low for the method to be used in clinical practice.

Regarding the shape accuracy, we reported mean unsigned distances between DXA and QCT-derived surfaces in a range between 1.37 mm and 1.72 mm at the total vertebra and between 0.63 mm and 0.68 mm at the vertebral body (Table I). Whitmarsh *et al.* [35] reported lower errors at the total vertebra (between 1.00 mm and 1.34 mm), but larger errors at the vertebral body (between 0.73 mm and 1.12 mm). We found similar correlation coefficients (R) for the vBMD. Our R-values ranged between 0.90 and 0.92 for the integral vBMD at the total vertebra, versus 0.86 and 0.93 in [35]. At the vertebral body, we achieved R-values between 0.82 and 0.85 (integral vBMD) and between 0.79 and 0.83 (trabecular vBMD) versus 0.80 and 0.89 (integral vBMD) and 0.82 and 0.90 (trabecular vBMD) in [35]. Reported results in [35] show lower errors in modelling the shape of the posterior processes, compared to our results, which can be explained using both AP and lateral DXA projection. However, a slightly lower accuracy in modelling the vertebral body shape was found. One important limitation of the method proposed in [35] is the use of the lateral DXA scans, which are not currently used in clinical practice. Moreover, no specific algorithm was proposed to quantify the cortical bone and L1 was not assessed. In Humbert *et al.* [31], a similar approach to the one proposed in our paper was developed for the proximal femur.

They reported R-values of 0.95, 0.85 and 0.94 (integral, trabecular and cortical vBMD) at the total femur, against 0.85, 0.83 and 0.84 at the L1-L4 segment vertebral bodies in our work. Regarding the CTh, they achieved an R-value of 0.92, against 0.83 in the present paper. The slightly lower accuracy reported in our work can be explained by the fact that the geometry of the spine is more complex than the one of the femur, the cortex is on average thinner in the vertebral body, compared to the total femur region of interest, and the spine DXA scans are noisier than hip DXA scans.

In the 180 subjects included in this study, bone masks and landmarks at L1-L4 segment (Fig. 3. "Bone Mask") automatically provided by the software of the DXA manufacturers were accurate enough to provide proper identification of the "L1-L4 Mask" (Fig. 3) to be used to initialize the statistical model and performed the registration. However, this process might fail, especially in the presence of pathologies such as severe scoliosis or severe osteoarthritis. In this case, manual input for the operator would be required to modify the data provided by the software of the DXA manufacturer prior to run the 2D/3D modelling process.

Modelling the outer and inner surfaces of the cortical shell was only performed in the vertebral body. The complex geometry of the back processes would make the segmentation of the cortical bone in this region of interest particularly challenging.

The lumbar vertebrae included in the training and validation databases are not only affected by bone density loss due to osteoporosis, but also by shape deformation due to degenerative osteoarthritis, compression, or the presence of calcifications (local accumulation of bone mineral) in the periphery of the vertebral body. Osteoarthritis is the most common of these conditions, with estimated rates as high as

40% in women older than 50 years, and 60% in those older than 70 years [47]. Our shape and density statistical model was mainly designed to capture global variations, while very local variations (as bone spurs, or osteophytes) were not included. Moreover, osteophytes are often not seen in the AP DXA scans. Therefore, the method proposed in our paper could hardly model local deformities, which is an important limitation. The accuracy in measuring the cortical bone volume and CTh is directly impacted by this limitation. Future work should consider the development of advanced statistical models for the lumbar spine, including articulated and/or multi-level model, which should be more accurate in modelling local deformations and the posterior arch of the vertebra.

The presence of osteoarthritis can also lead to a wrong diagnosis of the disease, since local accumulation of bone mineral at the periosteal surface might lead to an overestimation of the aBMD computed by DXA, and hence, to a higher T-score. In this sense, the DXA-derived 3D measurements of the trabecular bone at the vertebral body could provide an alternative measurement, overcoming this limitation by discarding bone spurs, local deformations at the periosteal surface, or in the back processes.

Our algorithm cannot model fractured vertebrae since the presence of fracture was an exclusion criterion for the subjects to be included to build the statistical model. This could, however, be handled by manually, or automatically, hiding the fractured vertebra(s) in the 2D mask to be used in the registration process. The L1-L4 model would be registered as described in Section II.C. The excluded region of interest (for example L3) would be statistically estimated based on the regions included (L1-L2-L4) and could be subsequently discarded in the following processing steps (cortical shell modelling, and clinical measurements). As future research, other measurements that could arise clinical interest in the lumbar spine should include: the intervertebral space, the lumbar curvature (so-called lordosis) and vertebral body heights, which are parameters associated to fracture risk.

V. CONCLUSION

To the best of our knowledge, the method proposed in this paper is the first attempt in the literature to estimate the 3D subject-specific shape and density of the lumbar spine from a single AP DXA scan, which makes it fully compatible with current clinical practices. We proposed a separate assessment of the cortical and the trabecular compartments, and gave special emphasis to the vertebral body, which is the most affected region by osteoporotic fractures. A very good agreement was found between the DXA-derived and QCT-derived clinical measurements that were evaluated in this paper. This method could potentially improve osteoporosis and fracture risk management in patients who had an AP DXA scan of the lumbar spine without any additional examination.

REFERENCES

[1] "Consensus Development Conference: Diagnosis, prophylaxis and treatment of osteoporosis," in *American Journal Medicine*, 1991, vol. 90, pp. 464–650.

[2] A. Svedbom, E. Hernlund, M. Ivergård, J. Compston, C. Cooper, J. Stenmark, E. V. McCloskey, B. Jönsson, and J. A. Kanis, "Osteoporosis in the European Union: A compendium of country-specific reports," *Arch. Osteoporos.*, vol. 8, no. 1–2, 2013.

[3] N. C. Harvey and E. V. McCloskey, "Gaps and solutions in bone health," *International Osteoporosis Foundation*. 2016.

[4] L. J. Melton, E. A. Chrischilles, C. Cooper, A. W. Lane, and B. L. Riggs, "Perspective. How many women have osteoporosis?," *J. Bone Miner. Res.*, vol. 7, no. 9, pp. 1005–1010, 1992.

[5] L. J. Melton, E. J. Atkinson, M. K. O'Connor, W. M. O'Fallon, and B. L. Riggs, "Bone Density and Fracture Risk in Men," *J. Bone Miner. Res.*, vol. 13, no. 12, pp. 1915–1923, 1998.

[6] J. A. Kanis, L. J. Melton, C. Christiansen, C. C. Johnston, and N. Khaltaev, "The diagnosis of osteoporosis," *J. Bone Miner. Res.*, vol. 9, no. 8, pp. 1137–1141, 1994.

[7] J. A. Kanis and WHO Scientific Group, "Assesment of osteoporosis at the primary health care level," *WHO Technical Report Series*. p. 339, 2007.

[8] ISCD, "Adult Official Positions of the International Society for Clinical Densitometry (ISCD)." 2015.

[9] H. K. Genant, C. Y. Wu, C. van Kuijk, and M. C. Nevitt, "Vertebral Fracture Assessment Using a Semiquantitative Technique," *J. Bone Miner. Res.*, vol. 8, no. 9, pp. 1137–1148, 1993.

[10] NIH Consensus Development Panel on Osteoporosis Prevention, "Osteoporosis: prevention, diagnosis, and management," *Am. J. Med.*, vol. 285, no. 6, pp. 785–95, 2001.

[11] L. J. Melton, E. J. Atkinson, W. M. O'Fallon, H. W. Wahner, and B. L. Riggs, "Long-term fracture prediction by bone mineral assessed at different skeletal sites," *J. Bone Miner. Res.*, vol. 8, no. 10, pp. 1227–1233, 1993.

[12] E. S. Siris, Y.-T. Chen, T. A. Abbott, E. Barrett-Connor, P. D. Miller, L. E. Wehren, and M. L. Berger, "Bone Mineral Density Thresholds for Pharmacological Intervention to Prevent Fractures," *Arch. Intern. Med.*, vol. 164, no. 10, pp. 1108–1112, 2004.

[13] B. C. Silva, S. B. Broy, S. Boutroy, J. T. Schousboe, J. A. Shepherd, and W. D. Leslie, "Fracture Risk Prediction by Non-BMD DXA Measures: the 2015 ISCD Official Positions Part 2: Trabecular Bone Score," *J. Clin. Densitom.*, vol. 18, no. 3, pp. 309–330, Jan. 2015.

[14] J. S. Bauer and T. M. Link, "Advances in osteoporosis imaging," *Eur. J. Radiol.*, vol. 71, no. 3, pp. 440–449, 2009.

[15] Y. Bala, R. Zebaze, and E. Seeman, "Role of cortical bone in bone fragility," *Curr. Opin. Rheumatol.*, vol. 27, no. 4, pp. 406–13, 2015.

[16] K. Engelke, J. E. Adams, G. Armbrecht, P. Augat, C. E. Bogado, M. L. Bouxsein, D. Felsenberg, M. Ito, S. Prevrhal, D. B. Hans, and E. M. Lewiecki, "Clinical Use of Quantitative Computed Tomography and Peripheral Quantitative Computed Tomography in the Management of Osteoporosis in Adults: The 2007 ISCD Official Positions," *J. Clin. Densitom.*, vol. 11, no. 1, pp. 123–162, 2008.

[17] T. D. Rachner, S. Khosla, and L. C. Hofbauer, "Osteoporosis: Now and the future," *Lancet*, vol. 377, no. 9773, pp. 1276–1287, 2011.

[18] S. Prevrhal, J. C. Fox, J. A. Shepherd, and H. K. Genant, "Accuracy of CT-based thickness measurement of thin structures: Modeling of limited spatial resolution in all three dimensions," *Med Phys*, vol. 30, no. 1, pp. 1–8, 2003.

[19] T. F. Cootes, "An Introduction to Active Shape Models," *Image Processing and Analysis*. Oxford University Press, pp. 223–248, 2000.

[20] T. F. Cootes, G. J. Edwards, and C. J. Taylor, "Active Appearance Models," in *European Conference on Computer Vision*, 1998, vol. 23, no. 6, pp. 681–685.

[21] M. Fleute and S. Lavallée, "Nonrigid 3-D/2-D registration of images using statistical models," in *MICCAI*, 1999, vol. LNCS1679, pp. 138–147.

[22] G. Zheng, S. Gollmer, S. Schumann, X. Dong, T. Feilkas, and M. Á. González Ballester, "A 2D/3D correspondence building method for reconstruction of a patient-specific 3D bone surface model using point distribution models and calibrated X-ray images," *Med. Image Anal.*, vol. 13, no. 6, pp. 883–899, 2009.

[23] N. Baka, B. L. Kaptein, M. de Bruijne, T. van Walsum, J. E. Giphart, W. J. Niessen, and B. P. F. Lelieveldt, "2D-3D shape reconstruction of the distal femur from stereo X-ray imaging using statistical shape models," *Med. Image Anal.*, vol. 15, no. 6, pp. 840–850, 2011.

[24] S. Benameur, M. Mignotte, S. Parent, H. Labelle, W. Skalli, and J.

A. De Guise, "3D/2D registration and segmentation of scoliotic vertebrae using statistical models," *Comput. Med. Imaging Graph.*, vol. 27, no. 5, pp. 321–337, 2003.

[25] J. Boisvert, F. Cheriet, X. Pennec, H. Labelle, and N. Ayache, "Articulated spine models for 3-D reconstruction from partial radiographic data," *IEEE Trans. Biomed. Eng.*, vol. 55, no. 11, pp. 2565–2574, 2008.

[26] L. Belenguer Querol, P. Büchler, D. Rueckert, L. P. Nolte, and M. Á. González Ballester, "Statistical finite element model for bone shape and biomechanical properties," in *MICCAI*, 2006, vol. 9, no. LNCS 4190, pp. 405–411.

[27] O. Ahmad, K. Ramamurthi, K. E. Wilson, K. Engelke, R. L. Prince, and R. H. Taylor, "Volumetric DXA (VXA): A new method to extract 3D information from multiple in vivo DXA images," *J. Bone Miner. Res.*, vol. 25, no. 12, pp. 2744–2751, 2010.

[28] T. Whitmarsh, L. Humbert, M. de Craene, L. M. del Río Barquero, A. F. Frangi, and M. De Craene, "Reconstructing the 3D shape and bone mineral density distribution of the proximal femur from dual-energy x-ray absorptiometry," *IEEE Trans. Med. Imaging*, vol. 30, no. 12, pp. 2101–2114, 2011.

[29] S. P. Väänänen, L. Grassi, G. Flivik, J. S. Jurvelin, and H. Isaksson, "Generation of 3D shape, density, cortical thickness and finite element mesh of proximal femur from a DXA image," *Med. Image Anal.*, vol. 24, pp. 125–134, 2015.

[30] T. N. Hangartner, "Thresholding technique for accurate analysis of density and geometry in QCT, pQCT and mCT images," *J. Musculoskelet. Neuronal Interact.*, vol. 7, no. 1, pp. 9–16, 2007.

[31] L. Humbert, Y. Martelli, R. Fonollà, M. Steghöfer, S. Di Gregorio, and L. M. Del Río Barquero, "3D-DXA: Assessing the Femoral Shape, the Trabecular Macrostructure and the Cortex in 3D from DXA images," *IEEE Trans. Med. Imaging*, vol. 36, no. 1, pp. 27–39, 2017.

[32] L. Humbert, J. Hazrati Marangalou, L. M. Del Río Barquero, G. H. van Lenthe, and B. van Rietbergen, "Technical Note: Cortical thickness and density estimation from clinical CT using a prior thickness-density relationship," *Med. Phys.*, vol. 43, no. 4, pp. 1945–1954, 2016.

[33] H. Chen, X. Zhou, H. Fujita, M. Onozuka, and K.-Y. Kubo, "Age-related changes in trabecular and cortical bone microstructure," *Int. J. Endocrinol.*, vol. 2013, p. 213234, 2013.

[34] H. Ritzel, M. Amling, M. Pösl, M. Hahn, and G. Delling, "The thickness of human vertebral cortical bone and its changes in aging and osteoporosis: a histomorphometric analysis of the complete spinal column from thirty-seven autopsy specimens.," *J. Bone Miner. Res.*, vol. 12, no. 1, pp. 89–95, 1997.

[35] T. Whitmarsh, L. Humbert, L. M. Del Río Barquero, S. Di Gregorio, and A. F. Frangi, "3D reconstruction of the lumbar vertebrae from anteroposterior and lateral dual-energy X-ray absorptiometry," *Med. Image Anal.*, vol. 17, no. 4, pp. 475–487, 2013.

[36] H. Hassanpour, N. Samadiani, and S. M. Mahdi Salehi, "Using morphological transforms to enhance the contrast of medical images," *Egypt. J. Radiol. Nucl. Med.*, vol. 46, no. 2, pp. 481–489, 2015.

[37] A. Top, G. Hamarneh, and R. Abugharbieh, "Spotlight: Automated confidence-based user guidance for increasing efficiency in interactive 3D image segmentation," in *MICCAI*, 2010, vol. 6533 LNCS, pp. 204–213.

[38] A. Top, G. Hamarneh, and R. Abugharbieh, "Active learning for interactive 3D image segmentation.," in *MICCAI*, 2011, vol. 14, pp. 603–10.

[39] A. Myronenko, X. Song, and M. Á. Carreira-Perpiñán, "Non-rigid point set registration: Coherent Point Drift," in *Neural Information Processing Systems*, 2007, vol. 19, pp. 1009–1016.

[40] A. Myronenko and X. Song, "Point-Set Registration: Coherent Point Drift," *IEEE Trans. Pattern Anal. Mach. Intell.*, vol. 32, no. 12, pp. 2262–2275, 2010.

[41] J. C. Gower, "Gerenalized Procrustes Analysis," *Psychometirka*, vol. 40, pp. 33–51, 1975.

[42] T. F. Cootes and C. J. Taylor, "Active Shape Models - 'Smart Snakes,'" in *British Machine Vision Conference*, 1992, no. 3, pp. 266–275.

[43] I. T. Jolliffe, *Principal Component Analysis*. 1986.

[44] T. F. Cootes, C. J. Taylor, D. H. Cooper, and J. Graham, "Active Shape Models-Their Training and Application," *Comput. Vis. Image Underst.*, vol. 61, no. 1, pp. 38–59, 1995.

[45] F. L. Bookstein, "Principal warps: Thin-Plate Splines and the decomposition of deformations," *IEEE Trans. Pattern Anal. Mach. Intell.*, vol. 11, no. 6, pp. 567–585, 1989.

[46] W. H. Press, B. Flannery, S. Teukolsky, and W. Vetterling, *Numerical recipes in C: The art of scienatic computing*. Cambridge University Press, 1992.

[47] D. L. Schneider, R. Bettencourt, and E. Barrett-Connor, "Clinical Utility of Spine Bone Density in Elderly Women," *J. Clin. Densitom.*, vol. 9, no. 3, pp. 255–260, 2006.